Circular RNA circRILPL1 promotes nasopharyngeal carcinoma malignant progression by activating the YAP/HIPPO signaling pathway

Pan Wu
Central South University
Xiangying Deng
Central South University
Yian Wang
Central South University
Chunmei Fan
Central South University
Xiangchan Hou
Central South University
Yongzhen Mo
Central South University
Yuming Wang
Central South University
Zheng Li
Central South University
Fuyan Wang
Central South University
Can Guo
Central South University
Ming Zhou
Central South University
Qianjin Liao
Central South University
Hui Wang
Central South University
Zhaoyang Zeng
Central South University
Weihong Jiang
Central South University
Guiyuan Li

Central South University

Bo Xiang

Central South University

Wei Xiong (xiongwei@csu.edu.cn)

Central South University

Research Article

Keywords: circRILPL1, nasopharyngeal carcinoma, YAP, ROCK1, IPO7

Posted Date: July 12th, 2022

DOI: https://doi.org/10.21203/rs.3.rs-1820853/v1

Abstract

Background

Circular RNAs (circRNAs) play an important regulatory role in the pathogenesis and progression of nasopharyngeal carcinoma (NPC), but they have not been sufficiently studied.

Methods

The high expression of circRILPL1 in NPC tissues was confirmed by quantitative real-time polymerase chain reaction (qRT-PCR) and *in situ* hybridization (ISH). The migration, invasion, proliferation, and mechanical properties of NPC cells were detected using wound healing, transwell, MTT, colony formation assays, and atomic force microscopy (AFM). Nude mice models including subcutaneous transplantation, tail vein-lung metastasis, and footpad-lymph node metastasis were established to determine the tumor-promoting effect of circRILPL1 *in vivo*. The proteomic analysis of circRILPL1 was performed by liquid chromatography coupled to tandem mass spectrometry (LC-MS/MS). The interaction of circRILPL1 with ROCK1 and IPO7 was verified through RNA pull-down, RNA immunoprecipitation (RIP) and immunofluorescence-fluorescence *in situ* hybridization (IF-FISH). The expression of the HIPPO pathway-related proteins was examined using western blotting. The nucleocytoplasmic distribution of YAP was analyzed by immunofluorescence and cytosolic/nuclear fractionation. The transcriptional activity of YAP was detected by luciferase reporter assay. The effect of circRILPL1 on the enrichment of YAP on CAPN2 and PXN promoters was examined by chromatin immunoprecipitation.

Results

We revealed for the first time that circRILPL1 was up-regulated in NPC, weakened adhesion and decreased stiffness of NPC cells, and promoted NPC proliferation and metastasis *in vitro* and *in vivo*. Mechanistically, circRILPL1 inhibited the LATS1-YAP kinase cascade by binding to and activating ROCK1, resulting in decrease of YAP phosphorylation and degradation. Binding to and cooperating with transport receptor IPO7, circRILPL1 promoted the translocation of YAP from the cytoplasm to the nucleus, where YAP promoted the transcription of cytoskeleton remodeling genes CAPN2 and PXN. By which, circRILPL1 contributed to the pathogenesis of NPC.

Conclusions

Our results demonstrated that circRILPL1 promoted the proliferation and metastasis of NPC through activating the YAP/HIPPO signaling pathway by binding to both ROCK1 and IPO7. Highly expressed circRILPL1 in NPC may serve as an important biomarker for tumor diagnosis and also may be a potential therapeutic target.

Introduction

Nasopharyngeal carcinoma (NPC) is a polygenic hereditary disease originating from nasopharyngeal epithelial cells. NPC is especially common in East and Southeast Asia with obvious regional clustering and ethnic predilection [1, 2]. Genetic components and environmental factors such as Epstein-Barr virus (EBV) infection are considered to be the cooperative pathogenic contributors of NPC, which exhibits strong tendency of local invasion and lymph node metastasis [3, 4]. However, during the pathogenesis of NPC, the oncogenic genomic changes and the relevant signaling processes remain far from clear [5–7].

Circular RNAs (circRNAs) are covalently closed non-coding RNAs formed by back-splicing at the 3' and 5' ends with lengths of hundreds or even thousands of bases. They have tissue-specific expression patterns, conserved and stable structures [8–11]. Studies have shown that circRNAs play important regulatory roles during tumorigenesis by acting as miRNA sponges, binding to proteins, and encoding small peptides [12–14]. CircSETD3 competitively adsorbs to miR-615-5p and miR-1538, thereby upregulating the expression of MAPRE1 [15]. CircARHGAP12 directly binds to the 3' UTR of EZR mRNA, promoting its stability [16]. CircPINT inhibits transcriptional elongation of multiple oncogenes in glioblastoma by encoding the small peptide PINT87aa [17]. In recent years, several unique circRNAs have been identified in NPC cells using high-throughput sequencing technology and bioinformatics technology. They are significantly differentially expressed between NPC cells and normal cells, closely correlated with NPC sizes, differentiation levels, lymph node and distant metastases, TNM stages, and overall survival rates [18, 19]. This suggests that circRNAs can be used as potential clinical diagnostic and prognostic indicators. However, the role they play and the underlying mechanism in the pathogenesis of NPC remain largely unknown.

In this study, we discovered that the circRNA circRILPL1 is highly expressed in NPC, which promotes NPC progression through activating the YAP/HIPPO signaling pathway. Mechanistically, circRILPL1 binds to and activates ROCK1 to inhibit the kinase LATS1, thereby inhibits the phosphorylation of YAP at Ser127 and Ser397 by LATS1, and enhances the YAP activity. Thereinto, circRILPL1 promotes YAP translocation into the nucleus by enhancing the interaction between YAP and IPO7, a nuclear transport receptor. In the nucleus, activated YAP promotes the transcription of CAPN2 and PXN. Through which, circRILPL1 was shown to promote the proliferation and metastasis of NPC *in vitro* and *in vivo*.

Materials And Methods

Patient samples

Two cohorts of NPC tissue samples were collected at Hunan Cancer Hospital, Changsha. The first cohort included 38 NPC tissues and 16 chronic nasopharyngeal inflammation tissues (Table S1) which were used for quantitative real-time polymerase chain reaction (qRT-PCR). The second cohort included 99 NPC tissues and 46 adjacent non-NPC tissues (Table S2) for *in situ* hybridization (ISH). This study was

approved by the Joint Ethics Committee of Central South University, and informed consents were obtained from all participants.

Cell culture and cell transfection

Cell lines (HNE2, CNE2, and HONE1) were obtained from the Cell Center of Central South University, and cultured in RPMI-1640 (Gibco, USA) containing 10% fetal bovine serum (Gibco, USA) at 37°C and 5% CO2.

The full-length circRILPL1 (hsa_circ_0007552) was amplified by PCR and then inserted into pcDNA3.1$^{(+)}$ circRNA Mini Vector, which was a gift from Professor Li Yong at Baylor College of Medicine. The YAP cDNA was cloned into pcDNA3.1$^{(+)}$. The construct for overexpression of IPO7 (IPO7 pcDNA3.1-3xFlag-C) was purchased from YouBio Company (Changsha, China). All constructs were confirmed by sequencing. Antisense oligonucleotides (ASO) specifically targeting circRILPL1, siRNAs targeting YAP, IPO7, and ROCK1 [20], and the controls were purchased from RiboBio Co., Ltd. (Guangzhou, China). The sequences for siRNA were listed in Table S3. Neofect (Neofect biotech Co., Ltd. China) was used for plasmid transfection. Hiperfect (Qiagen, Hilden, Germany) was used to transfect ASOs and siRNAs. The ROCK1 inhibitor Y-27632 (Selleck, Shanghai, China) was used in cells with a concentration of 10 uM.

RNA extraction and qRT-PCR

Total RNA was extracted from cells or tissues using TRIzol (Life, USA). Reverse transcription was performed using the HiScript cDNA Synthesis kit (Vazyme, Nanjing, China). Then, qRT-PCR was performed on CFX96™ Real-Time PCR Detection System using 2×SYBR Green qPCR Master Mix (Bimake, USA). All primers used were listed in Table S3.

Western blotting

RIPA buffer (Beyotime Biotechnology, Shanghai, China) and Protease Inhibitor cocktail (Roche Applied Sciences, Mannheim, Germany) were used for cell lysis and protein extraction. Protein samples (30-50 μg) were separated via 10-12% SDS-PAGE and transferred onto 0.2 μm PVDF membrane (Millipore, Billerica, MA, USA). After blocking with 5% nonfat milk for 1 h, the membrane was incubated with primary and secondary antibodies sequentially following the manufacturer's instruction. After washing with tris-buffered saline (TBS) or phosphate-buffered saline (PBS) supplemented with 0.1% Tween 20 for 3 times, the target protein bands were detected using the ECL detection system (Millipore, USA). Glyceraldehyde-3-phosphate dehydrogenase (GAPDH) was used as a loading control. All antibodies used are listed in Table S4.

RNase R and actinomycin D treatment

Actinomycin D (Sigma, USA) was added into NPC cells at a final concentration of 2 μg/ml, and RNA was collected at 0 h, 8 h, 16 h, and 24 h for qRT-PCR. For RNase R (RNR07250, Epicentre, USA) digestion, 20 U/μl RNase R was incubated with RNA extracted from NPC cells at 37°C for 30 min, and then the enzyme was inactivated by heating at 70°C for 10 min.

Cytosolic/nuclear fraction assay

Cytosolic and nuclear RNAs were isolated using the PARIS™ Protein and RNA Isolation System (Invitrogen, USA) following to the manufacturer's instructions. Cytosolic and nuclear proteins were separated using the NE-PER Nuclear and Cytoplasmic Extraction Reagent (Thermo Scientific, USA).

Immunohistochemistry (IHC) and *in situ* hybridization (ISH)

IHC was done using an immunohistochemical kit (KIT-9720, MXB Biotechnologies, Fuzhou, China). For ISH, digoxigenin-labeled circRILPL1-specific probes were synthesized by Sangon Biotech (Shanghai, China) and the expression of circRILPL1 in NPC tissue was detected specimens using the Enhanced Sensitive ISH Detection kit I (POD) (MK1030, BOSTER, China) following the manufacturer's instruction. The probes used were listed in Table S3. All sections were independently scored by two pathologists who were blind to the clinicopathological features of the samples (Table S2). A semi-quantitative scoring criterion was used based on the staining intensity and the proportion of positive cells. When the tissue was not stained, scoring 0. When the tissue was pale yellow, scoring 1; light brown, scoring 2; dark brown, scoring 3. On the other hand, when less than 25% of cells were positive, scoring 0; 25% - 50% positive, scoring 1; 50% - 75% positive, scoring 2; and more than 75% positive, scoring 3. Finally, a comprehensive score was calculated as the product of the staining intensity score and the positive ratio score. Scores greater than 5 were determined as high expression; others were considered as low expression.

RNA fluorescence *in situ* hybridization (FISH)

Cells were fixed with 4% paraformaldehyde and penetrated with 0.1% Triton-100. After incubation with pre-hybridization solution for 2-4 h at 37°C, cells were incubated with digoxigenin-labeled circRILPL1-specific probes (Sangon Biotech, China) at 37 °C overnight. After washing with SSC buffer, cells were incubated with biotinylated mouse anti-digoxigenin antibody for 1 h. Red fluorescence labeled mouse secondary antibody (LIFE, USA) was added at a dilution ratio of 1:200, and further incubated in the dark at 37°C for 1 h. DAPI (Invitrogen, USA) was added to counterstain the nuclei. Cells were imaged and analyzed using confocal microscope Ultra-View Vox (Perkin-Elmer, USA).

Wound healing and transwell assays

For wound healing assay, transfected cells were plated in 6-well plateand scratched evenly using sterilized mini tips. Then cells in each well were photographed and counted at 0 h and 24 h. For transwell assay, the diluted Matrigel (BD, Shanghai, China) was added to the upper chamber of Transwell chamber (Millipore, USA). Then transfected cells were added to the upper chamber and RPMI-1640 medium containing 20% FBS was added to the bottom chamber. Two days later, cells in the bottom chamber were photographed and counted using an inverted phase-contrast microscope after fixation and staining with 0.1% crystal violet.

MTT and colony formation assays

For MTT assay, 800 transfected cells were seeded in 96-well plates with 5 replicates in each group. After cell adhesion, 20 ul MTT (Beyotime, China) was added and incubated in the dark for 4 h at 37°C. Then, the plate was scanned at 490 nm using a microplate reader from day 0 to day 6. For colony formation assay, 2,000 transfected cells were seeded in 12-well plate and cultured for a week. The colonies in each well were photographed and counted after washing with PBS, fixation with 4% paraformaldehyde, and staining with 0.1% crystal violet.

Atomic Force Microscopy (AFM)

AFM (JPK NanoWizard 4 BioScience, JPK Instruments, Germany) was used to measure the biophysical properties of NPC cells. Cells were fixed in 2% glutaraldehyde for 45 s, 4% paraformaldehyde for 20 min, and then washed and maintained in appropriate amount of PBS for AFM scanning. The probe HYDRA6V-100NG (AppNano, CA, USA) with a spring constant of 0.292 N/m was used in the experiments. The indentation process was performed at a loading and retraction rate of approximately 2.5 μm/s with an indentation depth of at least 1 mm. Images were captured under QI mode, and analyzed with JPK software to obtain data on cell adhesion, stiffness, and Rq.

Immunofluorescence (IF)

Cells were fixed with pre-warmed 4% paraformaldehyde, penetrated with 0.1% Triton-100, and blocked with 5% calf serum albumin for 30 min at room temperature. Then cells were incubated with primary antibodies at 4°C overnight. After washing with PBS, they were incubated with fluorescently labeled secondary antibody (LIFE, USA) at 37°C for 1 h. Images were captured with laser confocal microscope Ultra-View Vox (Perkin-Elmer, USA) after counterstaining the nuclei with DAPI.

Luciferase reporter assay

Cells were co-transfected with the YAP luciferase reporter plasmid and the pRL-TK plasmid (which expresses Renilla luciferase as an internal control) after overexpression or knockdown of circRILPL1. The luciferase activity was measured using the Dual-Luciferase® Reporter Assay System (E1910, Promega, USA) 48 hours later. Relative luciferase activity was obtained by normalizing with the Renilla luciferase activity.

RNA immunoprecipitation (RIP) and chromatin immunoprecipitation (CHIP)

RIP was performed to analyze the interaction between circRILPL1 and ROCK1 or IPO7 using the Magna RIP^{TM} Kit (17-701, Millipore, USA) according to the manufacturer's instruction. CHIP was performed using the ChIP Assay Kit (P2078, Beyotime, China) following the manufacturer's instruction.

RNA pull-down

After transfection of biotin-labeled circRILPL1 probes for 24 hours, cells were lysed with the RIP buffer (150 mM KCl, 25 mM Tris-HCl, 0.5 mM DTT, 0.5% NP40) and incubated with 50 ul of Streptavidin

Dynabeads (M-280, Invitrogen, USA) overnight at 4°C with rotation. Then the RNA-protein complexes were examined by western blotting.

Immunoprecipitation

Cell lysates were incubated with antibodies (or the control IgG) and 50 ul of protein A/G magnetic beads (Bimake, Houston, Texas, USA) overnight at 4°C with rotation. After washing with GLB^+ buffer (10 mM NaCl, 10 mM Tris-HCl, 10 mM EDTA, 0.5% Triton-100) for 3 times, the precipitates were analyzed by western blotting.

Liquid chromatography coupled to tandem mass spectrometry (LC-MS/MS)

To identify circRILPL1 interacting proteins, cell lysates were incubated with biotin-labeled probes and biotin-affinity magnetic beads overnight at 4°C to pull down circRILPL1-associated proteins. The purified proteins were separated by SDS-PAGE gels and followed by liquid chromatography coupled to tandem mass spectrometry (LC-MS/MS) using Ultimate 3000 RSLC Nano System (Dionex, CA, USA) coupled with LTQ Orbitrap Velos Pro mass spectrometer (Thermo Scientific). Whole proteomic analysis was performed by searching the UniProt KB/Swiss-Prot database using the Proteome Discoverer 1.4 software. An fold change of $\geq$1.68 or $\leq$0.62 was used to define differentially expressed proteins.

Animal experiments

Female BALB/C nude mice were randomly divided into four groups. CNE2 cells (2×10^6) transfected with the vector, the circRILPL1 overexpression plasmid, antisense oligonucleotides against circRILPL1 (ASO-circRILPL1) or the scramble negative control were injected subcutaneously, via tail vein, or footpad, respectively. For the subcutaneous tumor model, mice (6 per group) were sacrificed 30 days after inoculation. The size of the subcutaneous tumor nodule was measured every 5 days and histological examinations were done after 30 days of inoculation. For the tail vein-lung metastasis model, mice were sacrificed 8 weeks after inoculation. The number and area of lung surface metastatic nodules in each mouse were recorded. The lungs were removed, imaged, and embedded in paraffin. Then, the tissues were sectioned for hematoxylin-eosin (H&E) staining, ISH experiments, and metastatic evaluation. For footpad-lymph node metastasis, mice were sacrificed 28 days after inoculation and the ipsilateral inguinal lymph nodes were excised for analysis. All experimental protocols involving animals were performed in accordance with the National Institutes of Health Guide for the Care and Use of Laboratory Animals and approved by the Institutional Animal Care and Use Committee of Central South University (Changsha, China).

Statistical analysis

Statistical analysis was performed using the GraphPad Prism 8.0. Student's t-test (two-tailed) to compare the difference between two groups of data. All data were represented as mean ± standard deviation (SD). P value < 0.05 was considered statistically significant.

Results

CircRILPL1 is highly expressed in NPC and associated with poor prognosis of NPC patients

To evaluate the role of circRNAs in the pathogenesis of NPC, we searched the RNA-seq dataset for NPC (GSE68799) in the GEO database, which including data from 4 chronically inflamed nasopharyngeal epithelial tissues and 41 NPC tissues. Extensive analysis identified 30 circRNAs with high expression in NPC tissues (Table S5), among which circRILPL1 (hsa_circ_0007552) that located on chromosome 12 (chr12:123983090-123984082) was not reported in NPC before (Fig. S1A). Results of qRT-PCR and sanger sequencing confirmed that it was formed by circular splicing of the exons 3 and 4 of the Rab interacting lysosomal protein like 1 (RILPL1) gene (NM_178314), with a total length of 341 bp (Fig. S1B). To examine the expression level of circRILPL1 in NPC, 38 NPC tissues and 16 chronic rhinitis epithelial tissues (as controls) were used for qRT-PCR, and the results showed that the expression of circRILPL1 was significantly elevated in NPC tissues than that in the controls (Fig. 1A). The results of ISH on paraffin sections of 99 NPCs and 46 non-cancer nasopharyngeal epithelial (NPE) tissues also confirmed that the expression of circRILPL1 in NPCs was significantly higher than that in the NPE samples. Importantly, Kaplan-Meier analysis revealed that the overall survival rate of patients with high circRILPL1 expression was lower than that of patients with low circRILPL1 expression (Fig. 1B). RNase R assays showed that circRILPL1 was more resistant to RNase R digestion than RILPL1 mRNA (Fig. 1C). Actinomycin D treatment further showed that the stability of circRILPL1 was much higher than that of RILPL1 linear mRNA (Fig. 1D), which is consistent with the stable circular RNA structure of circRILPL1. Results of RNA cytosolic/nuclear fraction assay and FISH showed that circRILPL1 was distributed both in the cytoplasm and the nucleus (Fig. 1E, F). All these data demonstrated that circRILPL1, a new circRNA that is highly expressed in NPC, may play a role in NPC tumorigenesis.

CircRILPL1 promotes the proliferation and metastasis of NPC cells, and alters the mechanical properties of NPC cells *in vitro*

To investigate the biological function of circRILPL1, circRILPL1 was overexpressed in NPC cell lines HNE2, CNE2, and HONE1 or its expression was knocked down using the specific ASO designed for circRILPL1 splice site (Fig. S2A). Wound healing and transwell assays showed that circRILPL1 could significantly enhance the migration and invasion of NPC cells (Fig. 2A-B, Fig. S2B). Cytoskeleton remodeling and pseudopod formation are closely associated with cancer invasion and metastasis. Immunofluorescence with phalloidin-labeled F-actin showed that overexpression of circRILPL1 promoted the polymerization of actin filaments, and knockdown of circRILPL1 resulted in reduced microfilaments and loss of cytoskeleton integrity in NPC cells (Fig. S2C). The process of carcinogenesis is also reflected by changes in the biophysical properties of cells [21]. Atomic force microscopy (AFM) showed that overexpression of circRILPL1 resulted in weakened adhesion and decreased stiffness of NPC cells, suggesting that cells were easier to detach from the surrounding tissues and their deformability was enhanced, consistent with the previously observed elevated capabilities of invasion and metastasis. And opposite results were obtained after knockdown of circRILPL1 (Fig. 2C, D). MTT and colony formation

experiments showed that overexpression of circRILPL1 promoted NPC cells proliferation, whereas knockdown of circRILPL1 inhibited the proliferation NPC cells (Fig. 2E, Fig. S2D). The above results indicated that circRILPL1 regulated the biophysical properties of NPC cells and promoted their proliferation, invasion, and migration *in vitro*.

CircRILPL1 promotes the proliferation and metastasis of NPC cells *in vivo*

To explore the tumor-promoting capability of circRILPL1 *in vivo*, xenograft models were established by injection of CNE2 cells transfected with circRILPL1 overexpression plasmid or ASO-circRILPL1 into 4-week-old nude mice. In the subcutaneous tumor model, tumor volume and tumor weight in the circRILPL1 overexpression group increased significantly compared to the that of the control group. In contrast, knockdown of circRILPL1 resulted in significantly lower tumor volume and weight (Fig. 3A, B). IHC data revealed that compared with the control the expression of Ki67 was higher in the circRILPL1 overexpression group and lower in the circRILPL1 knockdown group (Fig. 3C), indicating that circRILPL1 promoted NPC cells growth in mice. In the tail vein-lung metastasis model, the number and area of lung metastatic nodules were significantly increased in the circRILPL1 overexpression group while there were fewer and smaller lung metastatic nodules in the circRILPL1 knockdown group when compared with the control group (Fig. 3D-F), indicating that circRILPL1 significantly promoted lung metastasis of NPC cells in mice. Lymph node metastasis is a common spread of NPC [22, 23]. In the footpad-lymph node metastasis model, the inguinal lymph nodes were dissected and analyzed after 28 days as the tumor volume *in situ* gradually increased (Fig. S3A, B). The data showed weight and volume of metastatic inguinal lymph nodes in the circRILPL1 overexpression group were significantly higher than that in control group, whereas circRILPL1 knockdown produced the opposite effect (Fig. 3G, H). H&E staining confirmed that the area and number of metastatic tumor cells in lymph nodes were significantly increased after overexpression of circRILPL1, while there were fewer metastatic tumor cells in lymph nodes in the circRILPL1 knockdown group compared to the control group (Fig. 3I). All of these data demonstrated that circRILPL1 promoted NPC proliferation and metastasis *in vivo*.

CircRILPL1 activates the YAP/Hippo signaling pathway

To investigate the molecular mechanism underlying circRILPL1-mediated NPC proliferation and metastasis, the LC-MS/MS was performed for proteomic analysis in HNE2 cells after overexpression of circRILPL1 (Table S6). Bioinformatics analysis (https://david.ncifcrf.gov/) showed that 11 proteins in the Hippo signaling pathway were enriched (Table S7). Abnormality in the Hippo pathway leads to cancer development. The core of the Hippo pathway consists of a kinase cascade, kinases MST1/2 and LATS1/2, as well as their downstream effectors such as transcriptional coactivators YAP and TAZ [24, 25]. Phosphorylation of Ser127 and Ser397 inactivats YAP as Ser397 phosphorylation triggering its ubiquitination and proteasomal degradation, Ser127 phosphorylation mediating the interaction with 14-3-3 proteins and cytoplasmic retention [26]. Western blotting confirmed that phosphorylation of YAP (Ser127 and Ser397), total YAP, and phosphorylation of LATS1 were modulated in NPC cells by overexpression or knockdown of circRILPL1, with no significant effect on MST1 (Fig. 4A). While the

mRNA expression levels of them were not significantly altered (Fig. S4A). Cycloheximide (CHX) treatment and ubiquitination assays confirmed that circRILPL1 inhibited the ubiquitin-mediated degradation of YAP and increased its protein stability, leading to the upregulation of YAP protein level (Fig. 4B, C). Moreover, immunoprecipitation showed that circRILPL1 inhibited the binding of YAP to 14-3-3 (Fig. 4D). Cytosolic/nuclear protein fractionation assay and immunofluorescence staining further showed that circRILPL1 enhanced the abundance of YAP in nucleus while reduced the amount of YAP in cytoplasm, consistent with the inhibition of binding of YAP to 14-3-3 by circRILPL1 and also suggesting that circRILPL1 may function as a regulator for YAP-mediated transcription (Fig. 4E, Fig. S4B). The CTGF gene is a classical target gene of YAP, and the luciferase reporter assay revealed that overexpression of circRILPL1 significantly enhanced the transcriptional activity of YAP, while knockdown of circRILPL1 produced the opposite result (Fig. 4F). IHC data also confirmed that the expression of YAP was higher in the circRILPL1 overexpression group and lower in the circRILPL1 knockdown group in nude mice subcutaneous tumors and lung metastases tumors (Fig. S4C).

To test whether YAP participated in circRILPL1-mediated proliferation and migration of NPC cells, wound healing and transwell assays were performed and the results showed that overexpression of YAP partially restored the inhibitory effect of circRILPL1 knockdown on migration and invasion of NPC cells (Fig. 5A, B, Fig. S5A, B). AFM assays revealed that overexpression of YAP partially reversed the circRILPL1 knockdown-induced changes of cell biophysical properties (Fig. 5C, D). MTT and colony formation assays also showed the proliferation of NPC cells inhibited by ASO-circRILPL1 was reversed by overexpression of YAP (Fig. 5E, Fig. S5C). These data suggested that the function of circRILPL1 in NPC cells was dependent on activation of the YAP signaling pathway.

CircRILPL1 relieves LATS1-mediated YAP inhibition by binding to ROCK1

To explore the mechanism by which circRILPL1 regulates the YAP/HIPPO signaling pathway, RNA pull-down assay was performed and the result showed that circRILPL1 did not directly bind to LATS1 or YAP (Fig. S6A, B). Then, the RNA pull-down product was further analyzed by mass spectrometry and a total of 69 peptides were identified (Fig. 6A, Table S8). Rho associated coiled-coil containing protein kinase 1 (ROCK1) was selected for further analysis as it played important roles in tumorigenesis [27-29]. RNA pull-down assay confirmed the binding of circRILPL1 to ROCK1 (Fig. 6B). On the other hand, RIP assay showed that circRILPL1 was significantly enriched in the precipitated complex using anti-ROCK1 antibody compared to use IgG (Fig. 6C). The co-localization of circRILPL1 and ROCK1 was demonstrated by IF-FISH (Fig. 6D). The above data indicated that there was an interaction between circRILPL1 and ROCK1.

To investigate the role of ROCK1 in circRILPL1 regulated pathway, phosphorylation of Thr 696 on MYPT1, a well-known substrate of ROCK1 [30], was examined in NPC cells using western blotting after overexpression or knockdown of circRILPL1. The data showed that circRILPL1 promoted the phosphorylation of MYPT1 (Fig. 6E), but had no effect on the expression of ROCK1 at the protein and mRNA levels (Fig. 6E, Fig. S6C). The RhoA/Rock1 signaling regulates the YAP activity through LATS1 kinase [31]. Treatment with ROCK1 inhibitor Y27632 or siRNA targeting ROCK1 in NPC cells significantly

inhibited dephosphorylation of LATS1, which in turn inhibited dephosphorylation of YAP and resulted in decreased YAP protein level (Fig. S6D, E). When Y27632 or ROCK1 siRNA were used in circRILPL1-overexpressing NPC cells, the dephosphorylation of LATS1 and YAP, and the stability of YAP induced by circRILPL1 were significantly reduced (Fig. 6F, G). These results suggested that circRILPL1-mediated ROCK1 activation was critical for the regulation of LATS1-YAP kinase cascade. Transwell and MTT assays demonstrated that knockdown of ROCK1 partially reversed the promoting effects of circRILPL1 overexpression on the invasion and proliferation capabilities of of NPC cells (Fig. S6F, G). Together, these data demonstrated that ROCK1, as an important downstream effector of circRILPL1, is essential for the activation of YAP and promoting the proliferation and migration of NPC cells.

CircRILPL1 promotes YAP protein nuclear translocation by binding to IPO7

We noticed that in the mass spectrometry dataset following circRILPL1 pulled down , importin 7 (IPO7), is a nuclear transport receptor(Fig. S7A) [32, 33]. RNA pull-down, RIP assay, and IF-FISH confirmed the interaction between circRILPL1 and IPO7 (Fig. 7A-B, Fig. S7B). And immunoprecipitation showed that ROCK1 did not bind to IPO7 (Fig. S7C). To test whether circRILPL1 regulated the nuclear import of IPO7, cytosolic/nuclear subfrationation assay and immunofluorescence staining were performed and the results showed that overexpression of circRILPL1 induced IPO7 entering into nucleus and knockdown of circRILPL1 reduce its entry (Fig. 7C, Fig. S7D). Results of qRT-PCR and western blotting showed that circRILPL1 had no effect on the protein and mRNA expression of IPO7 (Fig. S7E, F). In addition, a weak interaction existed between endogenous IPO7 and YAP. But IPO7 did not regulate the expression and phosphorylation of YAP (Fig. S7G-I). Immunoprecipitation and immunofluorescence assay showed that the binding between IPO7 and YAP was significantly enhanced following overexpression of circRILPL1 (Fig. 7D, E). These results suggested that circRILPL1 mediated the binding between IPO7 and YAP. Notably, knockdown of IPO7 hindered circRILPL1-induced translocation of YAP from the cytoplasm to the nucleus and inhibited YAP transcriptional activity (Fig. 7F-G, Fig. S7J), indicating that circRILPL1 increasing the YAP nuclear import was partially IPO7-dependent. And this inhibition was more pronounced after simultaneous knockdown of IPO7 and ROCK1 (Fig. 7H).

CircRILPL1-YAP signaling promotes the transcription of CAPN2 and PXN

To search for key genes activated by the circRILPL1-YAP axis, the differentially expressed genes after circRILPL1 overexpression were analyzed by mass spectrometry, among which calpain 2 (CAPN2) and paxillin (PXN) were known to play important roles in cytoskeleton regulation, cell migration and invasion [34, 35]. Results of qRT-PCR and western blotting confirmed that circRILPL1 up-regulated the mRNA and protein expression of CAPN2 and PXN in NPC cells (Fig. 8A, B). Overexpression of YAP promoted the transcription of CAPN2 and PXN, while knockdown of YAP inhibited their transcription (Fig. S8A, B). Overexpression of YAP partially reversed the decrease of CAPN2 and PXN mRNA induced by circRILPL1 knockdown (Fig. 8C). ChIP experiment showed that circRILPL1 prompted the enrichment of YAP on the CAPN2 and PXN promoters in NPC cells (Fig. 8D). These results suggested that circRILPL1 promoted the transcription of CAPN2 and PXN through activation of YAP.

In summary, circRILPL1, as a tumor activator, bound to and activated ROCK1 to inhibit the LATS1 kinase, which leaded to decreased phosphorylation of YAP at Ser127 and Ser397 sites. Cooperating with nuclear transport receptor IPO7, circRILPL1 promoted YAP nuclear translocation by enhancing its interaction with IPO7. CircRILPL1 activated the YAP/HIPPO signaling pathway to promote the transcription of CAPN2 and PXN and NPC progression (Fig. 8E).

Discussion

CircRNAs are a new class of non-coding RNAs with covalently closed structure that have attracted much attention recently. CircRNAs regulate the occurrence and progression of a large variety of cancers [36]. For example, circRNF13 directly binds to and stabilizes SUMO2 mRNA and promotes GLUT1 degradation through SUMOylation and ubiquitination, thereby inhibiting the glycolysis [37]. EBV-encoded CircBART2.2 promotes the expression of PD-L1 in NPC cells by binding RIG-I and activating the transcription factors IRF3 and NF-κB, leading to tumor immune escape [38]. In this study, circRILPL1 was confirmed to reversely splice into a closed loop from the exons 3 and 4 of RILPL1 gene. RILPL1 can regulate cell morphology and polarity, and studies had shown that RILPL1 played an important role in LRRK2-mediated pathogenic interference with centrosomal cohesion and ciliogenesis [39, 40]. However, little is known about the roles of RILPL1 and in tumorigenesis. Previous studies showed that circRILPL1 could act as a sponge for miR-145 to activate IGF1R/PI3K/AKT signaling, thus promoting bovine muscle proliferation [41]. But the role of circRILPL1 in tumors has not been reported. Our study confirmed for the first time that the regulation of the proliferation and migration of NPC cells was dependent solely on circRILPL1, but not on RILPL1. The mechanical properties of cancer cells are determined by the cytoskeletal organization regulated by matrix stiffness, which can reflect their potential of malignant transformation, proliferation, and migration. Cells with different degrees of malignancy have different biophysical properties such as elasticity and adhesion tendency [42, 43]. Therefore, using AFM to integrate information such as adhesion, roughness, and stiffness of cancer cells can lead to a accurate understanding of cell structure and behavior, and prediction of canceration. Our work demonstrated that circRILPL1 reduced the adhesion and stiffness of NPC cells, making them prone to invasion and migration.

The Hippo pathway is an evolutionarily conserved signaling pathway that regulates cell morphology, proliferation, and migration. Regulation of the Hippo signaling by extracellular stimuli such as mechanical sensation or cell density affects the activity of YAP, which depends on LATS1/2-mediated direct phosphorylation of YAP [44]. Phosphorylation of Ser397 (annotated as Ser381 by Zhao et al. [45]) by LATS1/2 triggers β-TrCP-mediated YAP ubiquitination and proteasomal degradation, while YAP phosphorylation on Ser127 is essential for 14-3-3 binding and cytoplasmic retention [46]. The Hippo signaling pathway is rarely reported in NPC cells. Our data showed that circRILPL1 activated the YAP/Hippo signaling pathway through stabilizing YAP and facilitating its nuclear translocation, thereby transcriptionally activating the expression of cytoskeleton-remodeling and invasive metastasis relevant genes CAPN2 and PXN, ultimately promoting the malignant progression of NPC.

As a downstream effector of Rho, ROCK1 phosphorylates and regulates downstream protein kinase including MYPT, ERM, and LIMK to modulates actin polymerization. Actin and cytoskeleton could stimulate LATS1/2 kinase activity leading to YAP phosphorylation [47, 48]. Yang XM et al. found that RACGAP1 inhibited Hippo signaling and activated YAP in HCC cells by increasing the activity of RhoA, leading to polymerization of filamentous actin [49]. SPON2 regulated activities of RhoA and Rac1 through unique integrin signaling, affecting the F-actin reorganization, LATS1-Hippo pathway, and liver cancer cell migration [50]. Here we discovered circRILPL1 modulated the LATS1-YAP kinase cascade through binding to and activating ROCK1, resulting in the decreased YAP phosphorylation. However, the exact mechanism by which ROCK1 inhibited the kinase activity of LATS1 still needs further investigation.

IPO7 functions in protein nuclear import through acting as a nuclear transport receptor or as an adapter-like protein in association with the importin-beta subunit KPNB1 [51]. IPO7 usually binds to protein substrates containing nuclear localization signal (NLS) [52, 53]. A conserved bipartite NLS was identified in the N-terminal region of NUAK1, which is responsible for its nuclear import [54]. However, many proteins lacking the typical NLS have also been reported to undergo nuclear translocation. For instance, the sequence (Ser-Pro-Ser, SPS) in ERKs is phosphorylated upon stimulation. The phosphorylated ERK then binds to IPO7 and that leads to its nuclear translocation [55]. In addition, IPO7 has been reported responsible for nuclear import of plasmid DNA and human mitochondrial DNA. IPO7 may be a key pathway for nuclear import of DNA [56–58]. In this study, circRILPL1 was demonstrated to bind to IPO7 and drive the loading of YAP onto IPO7, thereby promoting the nuclear translocation of YAP, extending our understanding of circRILPL1-mediated YAP activation.

Collectively, we characterized a circRNA circRILPL1 playing a pivotal oncogenic role in NPC tumorigenesis through synergically regulating the activation of YAP and its nuclear translocation by binding to both ROCK1 and IPO7. This finding highlights the diagnostic and therapeutic potential of targeting circRILPL1 in NPC, uncovers a direct interaction between a circRNA and signaling proteins, and emphasizes the significance of circRNA functions in tumorigenesis and metastasis.

Abbreviations

CircRNA
circular RNA
NPC
nasopharyngeal carcinoma
NPE
nasopharyngeal epithelial
qRT-PCR
quantitative real-time polymerase chain reaction
ISH
in situ hybridization
IF

immunofluorescence
LC-MS/MS
Liquid chromatography coupled to tandem mass spectrometry
RIP
RNA immunoprecipitation
CHIP
chromatin immunoprecipitation
IF-FISH
immunofluorescence-fluorescence *in situ* hybridization
IHC
immunohistochemistry
H&E
hematoxylin-eosin
TNM
tumor (T), nodes (N), and metastases (M)
SD
Standard Deviation
ASO
Antisense oligonucleotides
AFM
Atomic force microscopy
CHX
cycloheximide
GAPDH
Glyceraldehyde-3-phosphate dehydrogenase
RILPL1
Rab Interacting Lysosomal Protein Like 1
ROCK1
Rho Associated Coiled-Coil Containing Protein Kinase 1
IPO7
importin 7
CTGF
connective tissue growth factor
NLS
nuclear localization signal

Declarations

Ethics approval and consent to participate

The present study was approved by the Ethics Committee of Central South University.

Consent for publication

Not applicable.

Availability of data and material

All data that support the findings of this study are available from the corresponding authors upon reasonable request.

Competing interests

The authors declare that they have no competing interests.

Funding

This study was funded by the National Natural Science Foundation of China (U21A20382, 82073135, 82072374, and 82002239), the Overseas Expertise Introduction Project for Discipline Innovation (111 Project, No. 111-2-12), the Natural Science Foundation of Hunan Province (2020JJ4125).

Authors' contributions

Wei Xiong and Bo Xiang conceived and designed the project. Pan Wu completed the majority of experiments and wrote the manuscript. Xiangying Deng, Yian Wang, Chunmei Fan, Xiangchan Hou, Yongzhen Mo, Yumin Wang, Zheng Li performed some of the experiments. Fuyan Wang, Can Guo, Ming Zhou, Zhaoyang Zeng and Guiyuan Li revised the manuscript. Qianjin Liao, Hui Wang and Weihong Jiang collected tissue samples. Wei Xiong and Bo Xiang is responsible for research supervision and funding acquisition. All authors read and approved the final manuscript.

Acknowledgements

We thank Prof. Yong Li for providing pcDNA3.1$^{(+)}$ CircRNA Mini Vectors.

References

1. Chen, Y.P., et al., *Nasopharyngeal carcinoma*. Lancet, 2019. **394**(10192): p. 64–80.
2. Wong, K.C.W., et al., *Nasopharyngeal carcinoma: an evolving paradigm*. Nat Rev Clin Oncol, 2021.
3. Chua, M.L.K., et al., Nasopharyngeal carcinoma. Lancet, 2016. **387**(10022): p. 1012–1024.
4. Xiong, W., et al., *A susceptibility locus at chromosome 3p21 linked to familial nasopharyngeal carcinoma*. Cancer Res, 2004. **64**(6): p. 1972–4.
5. Kang, Y., et al., *Advances in targeted therapy mainly based on signal pathways for nasopharyngeal carcinoma*. Signal Transduct Target Ther, 2020. **5**(1): p. 245.
6. Lin, D.C., et al., *The genomic landscape of nasopharyngeal carcinoma*. Nat Genet, 2014. **46**(8): p. 866–71.

7. Zeng, Z., et al., *Nasopharyngeal carcinoma: advances in genomics and molecular genetics*. Sci China Life Sci, 2011. **54**(10): p. 966–75.
8. Chen, I., C.Y. Chen, and T.J. Chuang, *Biogenesis, identification, and function of exonic circular RNAs*. Wiley Interdiscip Rev RNA, 2015. **6**(5): p. 563–79.
9. Guo, J.U., et al., *Expanded identification and characterization of mammalian circular RNAs*. Genome Biol, 2014. **15**(7): p. 409.
10. He, A.T., et al., *Targeting circular RNAs as a therapeutic approach: current strategies and challenges*. Signal Transduct Target Ther, 2021. **6**(1): p. 185.
11. Qu, S., et al., *Circular RNA: A new star of noncoding RNAs*. Cancer Lett, 2015. **365**(2): p. 141–8.
12. Kristensen, L.S., et al., *Circular RNAs in cancer: opportunities and challenges in the field*. Oncogene, 2018. **37**(5): p. 555–565.
13. Yang, Z., et al., *Circular RNAs: Regulators of Cancer-Related Signaling Pathways and Potential Diagnostic Biomarkers for Human Cancers*. Theranostics, 2017. **7**(12): p. 3106–3117.
14. Zhou, W.Y., et al., *Circular RNA: metabolism, functions and interactions with proteins*. Mol Cancer, 2020. **19**(1): p. 172.
15. Tang, L., et al., *circSETD3 regulates MAPRE1 through miR-615-5p and miR-1538 sponges to promote migration and invasion in nasopharyngeal carcinoma*. Oncogene, 2021. **40**(2): p. 307–321.
16. Fan, C., et al., *CircARHGAP12 promotes nasopharyngeal carcinoma migration and invasion via ezrin-mediated cytoskeletal remodeling*. Cancer Lett, 2021. **496**: p. 41–56.
17. Zhang, M., et al., *A peptide encoded by circular form of LINC-PINT suppresses oncogenic transcriptional elongation in glioblastoma*. Nat Commun, 2018. **9**(1): p. 4475.
18. Yang, M. and W. Huang, *Circular RNAs in nasopharyngeal carcinoma*. Clin Chim Acta, 2020. **508**: p. 240–248.
19. Zhou, D.N., et al., *Integrated analysis of transcriptome profiling predicts potential lncRNA and circRNA targets in human nasopharyngeal carcinoma*. Oncol Lett, 2020. **19**(4): p. 3123–3136.
20. Tang, H., et al., *Upregulated expression of ROCK1 promotes cell proliferation by functioning as a target of miR-335-5p in non-small cell lung cancer*. J Cell Physiol, 2019.
21. Deng, X., et al., *Application of atomic force microscopy in cancer research*. J Nanobiotechnology, 2018. **16**(1): p. 102.
22. Ho, F.C., et al., *Patterns of regional lymph node metastasis of nasopharyngeal carcinoma: a meta-analysis of clinical evidence*. BMC Cancer, 2012. **12**: p. 98.
23. Hong, X., et al., *Circular RNA CRIM1 functions as a ceRNA to promote nasopharyngeal carcinoma metastasis and docetaxel chemoresistance through upregulating FOXQ1*. Mol Cancer, 2020. **19**(1): p. 33.
24. Meng, Z., T. Moroishi, and K.L. Guan, *Mechanisms of Hippo pathway regulation*. Genes Dev, 2016. **30**(1): p. 1–17.

25. Zhao, B., K. Tumaneng, and K.L. Guan, *The Hippo pathway in organ size control, tissue regeneration and stem cell self-renewal*. Nat Cell Biol, 2011. **13**(8): p. 877–83.
26. Zanconato, F., M. Cordenonsi, and S. Piccolo, *YAP/TAZ at the Roots of Cancer*. Cancer Cell, 2016. **29**(6): p. 783–803.
27. Hu, C., et al., *ROCK1 promotes migration and invasion of nonsmallcell lung cancer cells through the PTEN/PI3K/FAK pathway*. Int J Oncol, 2019. **55**(4): p. 833–844.
28. Jerrell, R.J. and A. Parekh, *Matrix rigidity differentially regulates invadopodia activity through ROCK1 and ROCK2*. Biomaterials, 2016. **84**: p. 119–129.
29. Wang, Y., et al., *Long noncoding RNA DANCR, working as a competitive endogenous RNA, promotes ROCK1-mediated proliferation and metastasis via decoying of miR-335-5p and miR-1972 in osteosarcoma*. Mol Cancer, 2018. **17**(1): p. 89.
30. Boyle, S.T., et al., *ROCK-mediated selective activation of PERK signalling causes fibroblast reprogramming and tumour progression through a CRELD2-dependent mechanism*. Nat Cell Biol, 2020. **22**(7): p. 882–895.
31. Li, Q., et al., *MYBL2 disrupts the Hippo-YAP pathway and confers castration resistance and metastatic potential in prostate cancer*. Theranostics, 2021. **11**(12): p. 5794–5812.
32. Yao, X., et al., *Preferential utilization of Imp7/8 in nuclear import of Smads*. J Biol Chem, 2008. **283**(33): p. 22867–74.
33. Ju, J.H., et al., *Regulation of cell proliferation and migration by keratin19-induced nuclear import of early growth response-1 in breast cancer cells*. Clin Cancer Res, 2013. **19**(16): p. 4335–46.
34. Kakurina, G.V., et al., *Relationship between the mRNA Expression Levels of Calpains 1/2 and Proteins Involved in Cytoskeleton Remodeling*. Acta Naturae, 2020. **12**(1): p. 110–113.
35. Liu, S.C., et al., *Cytoplasmic LIF reprograms invasive mode to enhance NPC dissemination through modulating YAP1-FAK/PXN signaling*. Nat Commun, 2018. **9**(1): p. 5105.
36. Wang, Y., et al., *Circular RNAs in human cancer*. Mol Cancer, 2017. **16**(1): p. 25.
37. Mo, Y., et al., *Circular RNA circRNF13 inhibits proliferation and metastasis of nasopharyngeal carcinoma via SUMO2*. Mol Cancer, 2021. **20**(1): p. 112.
38. Ge, J., et al., *Epstein-Barr virus-encoded circular RNA circBART2.2 promotes immune escape of nasopharyngeal carcinoma by regulating PD-L1*. Cancer Res, 2021.
39. Sobu, Y., et al., *Pathogenic LRRK2 regulates ciliation probability upstream of tau tubulin kinase 2 via Rab10 and RILPL1 proteins*. Proc Natl Acad Sci U S A, 2021. **118**(10).
40. Lara Ordonez, A.J., et al., *RAB8, RAB10 and RILPL1 contribute to both LRRK2 kinase-mediated centrosomal cohesion and ciliogenesis deficits*. Hum Mol Genet, 2019. **28**(21): p. 3552–3568.
41. Shen, X., et al., *CircRILPL1 promotes muscle proliferation and differentiation via binding miR-145 to activate IGF1R/PI3K/AKT pathway*. Cell Death Dis, 2021. **12**(2): p. 142.
42. Kwon, T., S. Gunasekaran, and K. Eom, *Atomic force microscopy-based cancer diagnosis by detecting cancer-specific biomolecules and cells*. Biochim Biophys Acta Rev Cancer, 2019. **1871**(2): p. 367–

378.

43. Deng, X., et al., *LncRNA LINC00472 regulates cell stiffness and inhibits the migration and invasion of lung adenocarcinoma by binding to YBX1*. Cell Death Dis, 2020. **11**(11): p. 945.
44. Ma, S., et al., *The Hippo Pathway: Biology and Pathophysiology*. Annu Rev Biochem, 2019. **88**: p. 577–604.
45. Zhao, B., et al., *A coordinated phosphorylation by Lats and CK1 regulates YAP stability through SCF(beta-TRCP)*. Genes Dev, 2010. **24**(1): p. 72–85.
46. Zhao, T., et al., *HTLV-1 activates YAP via NF-kappaB/p65 to promote oncogenesis*. Proc Natl Acad Sci U S A, 2022. **119**(9).
47. Zhao, B., et al., *Cell detachment activates the Hippo pathway via cytoskeleton reorganization to induce anoikis*. Genes Dev, 2012. **26**(1): p. 54–68.
48. Chang, Y.C., et al., *Hippo Signaling-Mediated Mechanotransduction in Cell Movement and Cancer Metastasis*. Front Mol Biosci, 2019. **6**: p. 157.
49. Yang, X.M., et al., *Overexpression of Rac GTPase Activating Protein 1 Contributes to Proliferation of Cancer Cells by Reducing Hippo Signaling to Promote Cytokinesis*. Gastroenterology, 2018. **155**(4): p. 1233–1249 e22.
50. Zhang, Y.L., et al., *SPON2 Promotes M1-like Macrophage Recruitment and Inhibits Hepatocellular Carcinoma Metastasis by Distinct Integrin-Rho GTPase-Hippo Pathways*. Cancer Res, 2018. **78**(9): p. 2305–2317.
51. Xue, J., et al., *Forkhead Box M1 Is Essential for Nuclear Localization of Glioma-associated Oncogene Homolog 1 in Glioblastoma Multiforme Cells by Promoting Importin-7 Expression*. J Biol Chem, 2015. **290**(30): p. 18662–70.
52. Chen, J., et al., *Nuclear import of early growth response-1 involves importin-7 and the novel nuclear localization signal serine-proline-serine*. Int J Biochem Cell Biol, 2011. **43**(6): p. 905–12.
53. Panagiotopoulos, A.A., et al., *The sequence [EKRKI(E/R)(K/L/R/S/T)] is a nuclear localization signal for importin 7 binding (NLS7).* Biochim Biophys Acta Gen Subj, 2021. **1865**(5): p. 129851.
54. Palma, M., et al., *Identification of a nuclear localization signal and importin beta members mediating NUAK1 nuclear import inhibited by oxidative stress*. J Cell Biochem, 2019. **120**(9): p. 16088–16107.
55. Chuderland, D., A. Konson, and R. Seger, *Identification and characterization of a general nuclear translocation signal in signaling proteins*. Mol Cell, 2008. **31**(6): p. 850–61.
56. Dhanoya, A., et al., *Importin-7 mediates nuclear trafficking of DNA in mammalian cells*. Traffic, 2013. **14**(2): p. 165–75.
57. Miller, A.M., et al., *Identification of protein cofactors necessary for sequence-specific plasmid DNA nuclear import*. Mol Ther, 2009. **17**(11): p. 1897–903.
58. Zaitseva, L., et al., *HIV-1 exploits importin 7 to maximize nuclear import of its DNA genome*. Retrovirology, 2009. **6**: p. 11.

Figures

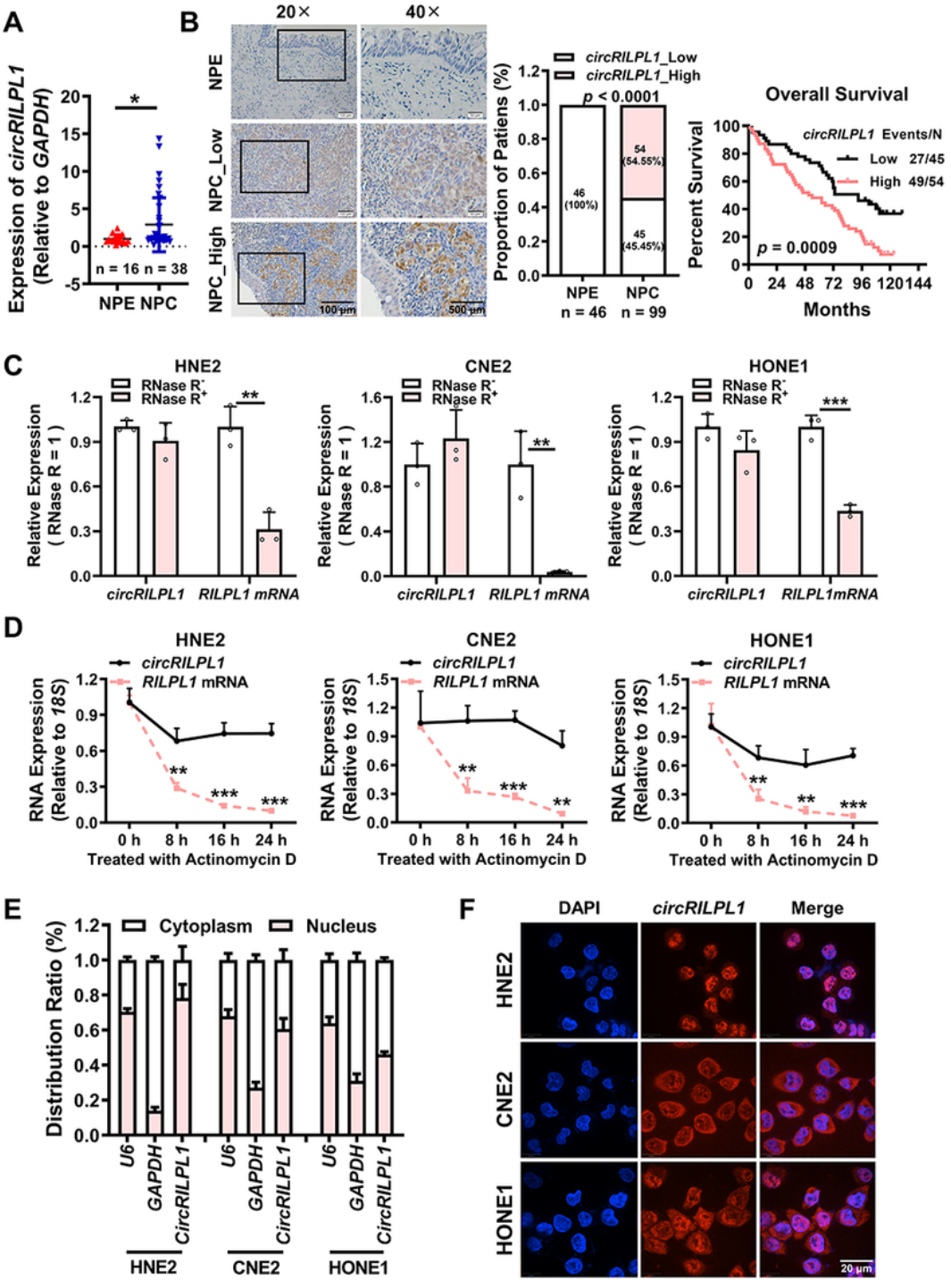

Figure 1

CircRILPL1 is highly expressed in NPC and associated with poor prognosis of NPC patients.

A The differential expression of circRILPL1 in 16 chronic rhinitis epithelial tissues and 38 NPC tissues was detected by qRT-PCR. *, $p < 0.05$. **B** CircRILPL1 was highly expressed and correlated with the prognosis of NPC patients in 99 NPC paraffin tissue sections, compared with 46 adjacent non-cancerous NPEs by ISH. Left, representative images of ISH. Magnification: 200×, Scale bar = 100 μm; Magnification: 400×, Scale bar = 50 μm. Middle, statistical analysis of ISH scores. Right, Kaplan-Meier survival analysis showed that the overall survival rate of NPC patients with high circRILPL1 expression was significantly lower than that of NPC patients with low circRILPL1 expression, $p = 0.0009$. **C** The relative expression levels of circRILPL1 and RILPL1 mRNA in NPC cells were detected after treating with RNase R for 30 min. 18S RNA was used as an internal reference. **, $p < 0.01$; ***, $p < 0.001$. **D** The relative expression levels of circRILPL1 and RILPL1 mRNA in NPC cells were detected after treating with actinomycin D for 0 h, 8 h, 16 h, and 24 h. 18S RNA was used as an internal reference. **, $p < 0.01$; ***, $p < 0.001$. **E** The intracellular localization of circRILPL1 was detected by RNA cytoplasm/nucleus fractionation assay. U6 was used as the nuclear internal reference, and GAPDH was used as the cytoplasmic internal control. **F** The intracellular localization of circRILPL1 was detected by FISH in NPC cells. Nuclei were stained with DAPI (blue). Scale bar = 20 μm. Data are presented as the means ± SD.

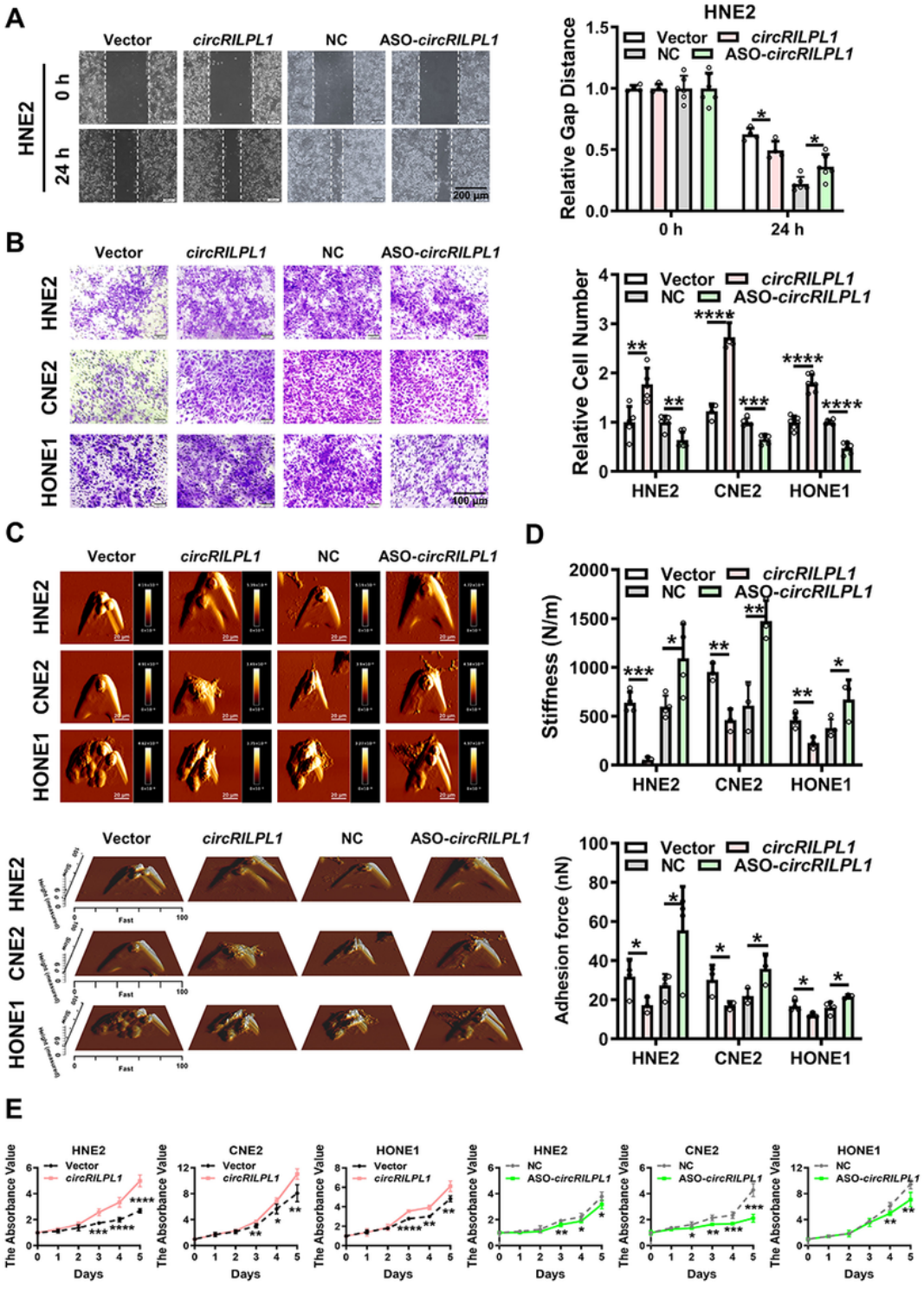

Figure 2

CircRILPL1 promotes NPC cells migration, invasion and proliferation and alters the mechanical properties of NPC cells *in vitro*.

A The migration ability of circRILPL1 was examined in HNE2 cells after overexpression or knockdown of circRILPL1 by wound healing assay. Images were acquired at 0 and 24 h. Scale bars = 200 μm. **B** The

invasion ability of circRILPL1 was assessed in HNE2, CNE2, and HONE1 cells after overexpression or knockdown of circRILPL1 by transwell assay. Images were acquired at 48 h. Scale bars =100 μm. **C** Representative AFM deflection images (top) and representative three-dimensional height distribution images (bottom) of NPC cells. **D** The stiffness (N/m) and adhesion force (nN) of NPC cells were measured and analyzed using JPK image processing software. **E** The effect of circRILPL1 on NPC cells proliferation was evaluated in HNE2, CNE2, and HONE1 cells after overexpression or knockdown of circRILPL1 by MTT assay. All data are presented as the means ± SD. *, $p < 0.05$; **, $p < 0.01$; ***, $p < 0.001$; ****, $p < 0.0001$.

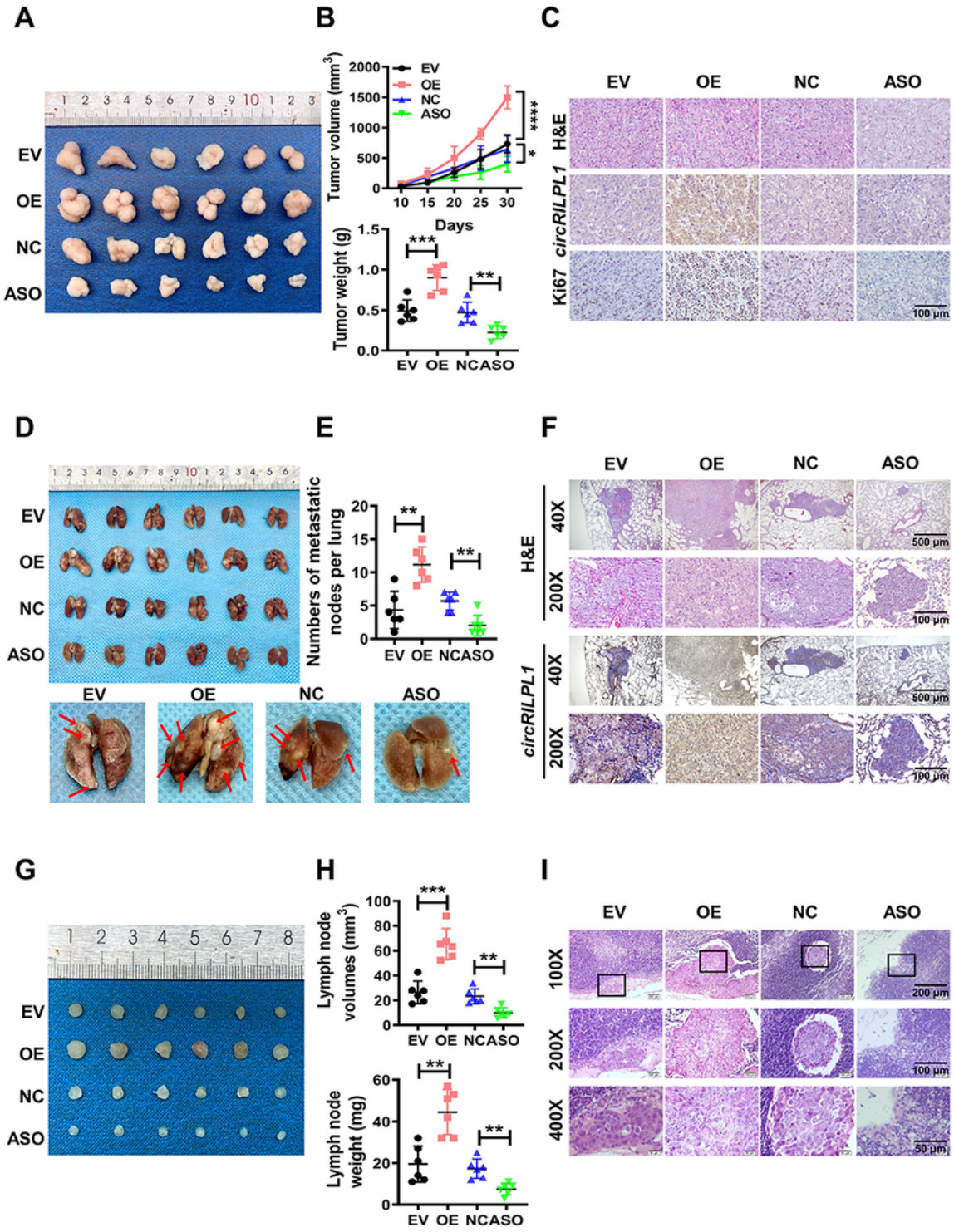

Figure 3

CircRILPL1 promotes the proliferation and metastasis of NPC cells *in vivo*.

CNE2 cells (2×10^6) transfected with the empty vector, the circRILPL1 overexpression plasmid, antisense oligonucleotides against circRILPL1 (ASO-circRILPL1), or the scramble negative control were injected subcutaneously, through the tail vein, or footpad of nude mice (n = 6 per group). **A** Representative images

of subcutaneous tumor tissues (n = 6 per group). **B** The tumor volume growth curves (top) and the tumor weights (bottom) of subcutaneous tumors in nude mice. *, $p < 0.05$; **, $p < 0.01$; ***, $p < 0.001$; ****, $p < 0.0001$. **C** Representative images of H&E staining, circRILPL1 staining, and Ki67 staining of subcutaneous tumors. Paraffin-embedded and sectioned subcutaneous tumors were subjected to H&E staining, ISH for circRILPL1 expression, and IHC for Ki67 expression. Magnification: 200×, scale bar = 100 μm. **D** Representative images of lung tissues dissected from nude mice (top, n = 6 per group). Representative images of metastatic nodules on the lung surface as indicated by arrows (bottom). **E** Quantification of the number of metastatic nodes in the lungs. **, $p < 0.01$. **F** Representative images of H&E staining of metastatic lung lesions and the expression of circRILPL1 by ISH assay. Magnification: 40×, scale bar = 500 μm; Magnification: 200×, scale bar = 100 μm. **G** Images of inguinal lymph nodes dissected from nude mice 28 days after injection via footpad (n = 6 per group). **H** The volume (top) and weight (bottom) of lymph nodes were measured for each group. **, $p < 0.01$; ***, $p < 0.001$. **I** Representative images of H&E staining of inguinal lymph nodes showing metastatic tumor cells. Magnification: 100×, scale bar = 200 μm; Magnification: 200×, scale bar = 100 μm; Magnification: 400×, scale bar = 50 μm. Data are presented as the means ± SD.

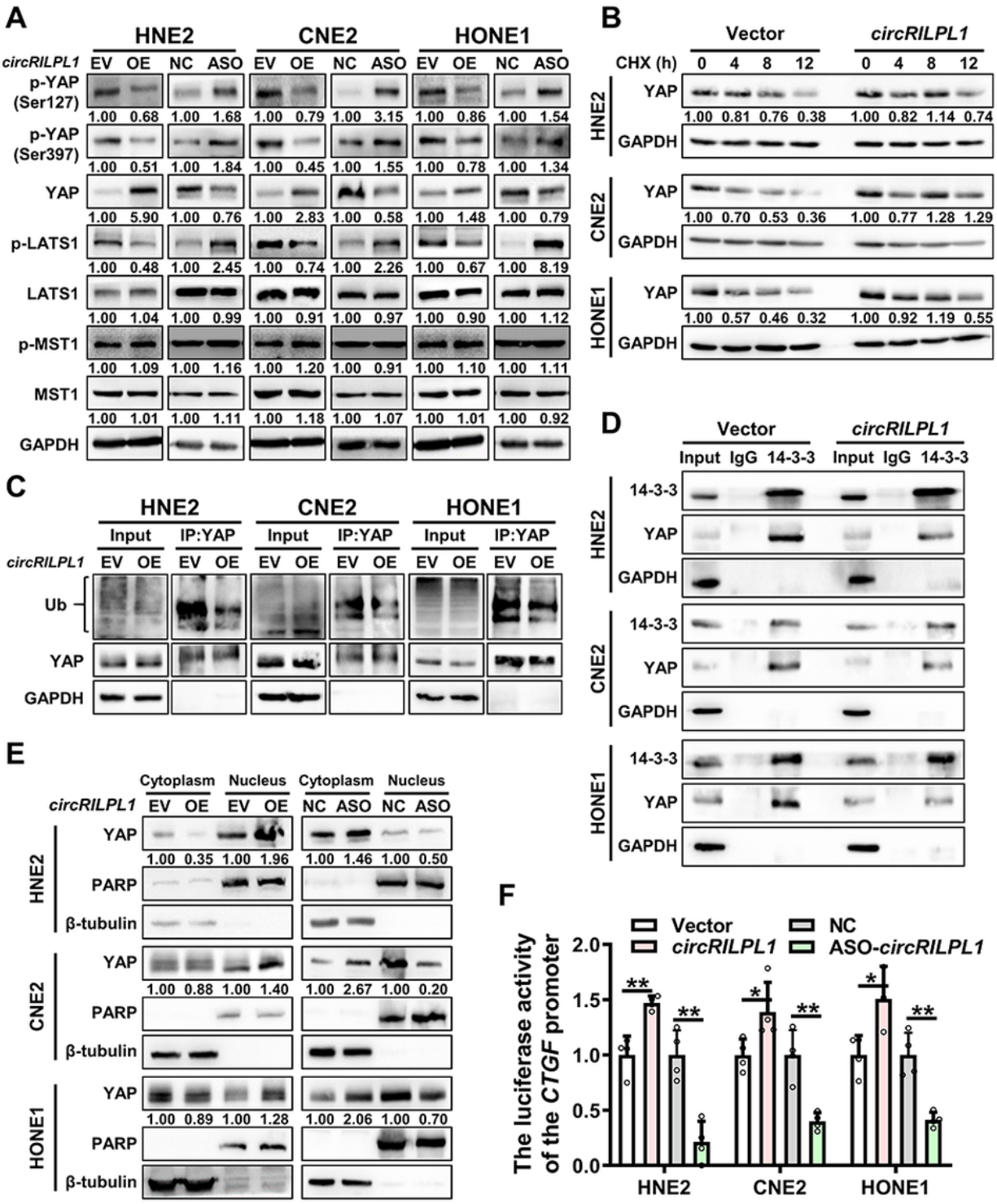

Figure 4

CircRILPL1 activates the YAP/Hippo signaling pathway.

A The effect of circRILPL1 on the expression level of key proteins of the Hippo signaling pathway was examined by western blotting in NPC cells. **B** The degradation of YAP protein was determined by western blotting in NPC cells treated with cycloheximide (CHX, 50 μg/mL) after overexpression of circRILPL1. **C**

The effect of circRILPL1 on the ubiquitination level of YAP protein was detected in NPC cells treated with MG132 for 12 h after overexpression of circRILPL1plasmid for 48 h. Cell lysates were subjected to immunoprecipitation using anti-YAP antibody followed by western blotting using anti-ubiquitin antibody. **D** The interaction between YAP and 14-3-3 proteins in NPC cells after overexpression of circRILPL1 was detected by immunoprecipitation using anti-14-3-3 antibody, followed by western blotting using YAP antibody. GAPDH was used as a negative control. **E** The abundance of YAP protein in nucleus and cytoplasm was examined in NPC cells after overexpression or knockdown of circRILPL1. PARP was used as a nuclear marker and β-tubulin as a cytoplasmic marker. **F** The result of CTGF luciferase reporter assay showed that circRILPL1 increased the transcriptional activity of YAP. *, $p < 0.05$; **, $p < 0.01$. Data are presented as the means ± SD.

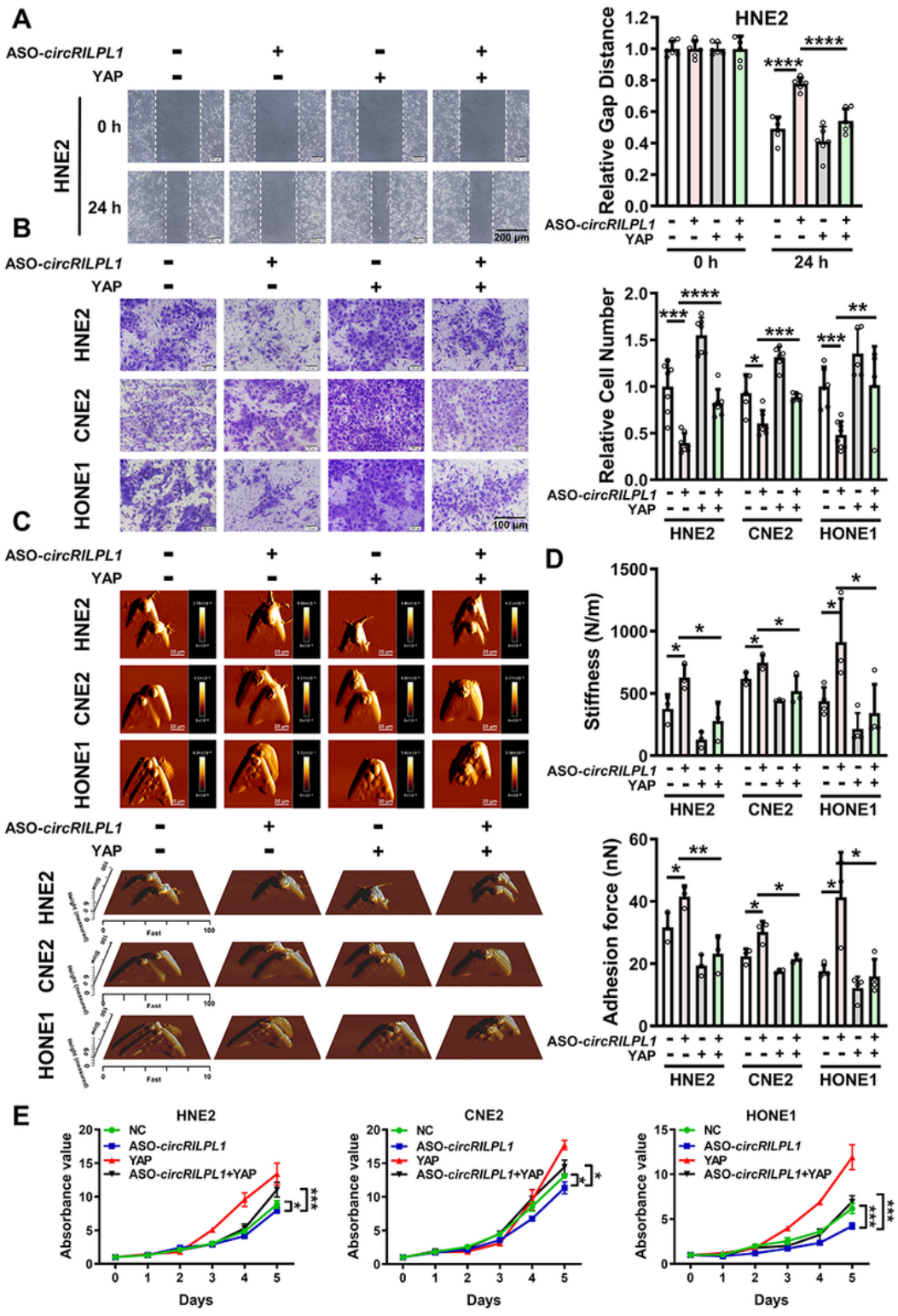

Figure 5

CircRILPL1 regulates NPC cells proliferation, migration, invasion and mechanical properties through YAP signaling.

Wound healing assay (**A**), transwell assay (**B**), AFM assay (**C, D**), and MTT assay (**E**) were performed to assess the effect of YAP on NPC cells migration, invasion, biophysical properties, and proliferation that

regulated by circRILPL1. Data are presented as the means ± SD. *, p < 0.05; **, p < 0.01; ***, p < 0.001; ****, p < 0.0001.

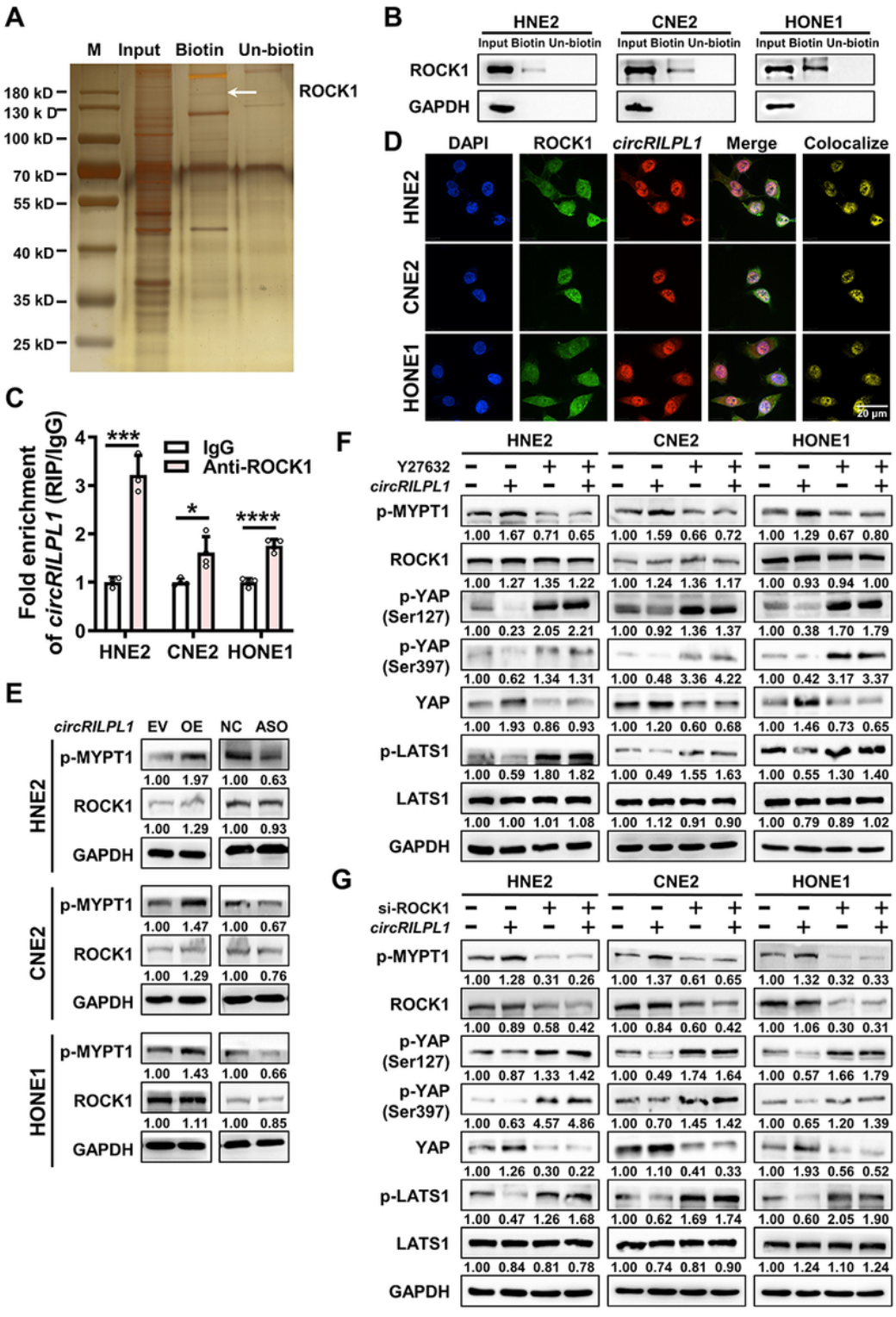

Figure 6

CircRILPL1 inhibits the LATS1-YAP kinase cascade by binding to ROCK1.

A The proteins pulled-down by circRILPL1 were separated by the SDS-PAGE, followed by silver staining and identification by LC-MS/MS. Biotin: biotinylated probe targeting the circRILPL1 back-spliced site; Un-biotin: unbiotinylated probe, as control. ROCK1(158 kDa) was also identified. **B** The interaction between circRILPL1 and ROCK1 protein was detected in NPC cells using RNA pull-down assay with a biotin-labeled circRILPL1 probe. GAPDH was used as a negative control. **C** The interaction between circRILPL1 and ROCK1 protein was detected in NPC cells by RIP assay using anti-ROCK1 antibody. The fold enrichment of circRILPL1 was relative to that of the control IgG. Data were are presented as the means ± SD. *, $p < 0.05$; ***, $p < 0.001$; ****, $p < 0.0001$. **D** The co-localization between circRILPL1 and ROCK1 protein was detected by IF-FISH. DAPI: blue; ROCK1: green; CircRILPL1: red; Scale bar = 20 μm. **E** The effects of circRILPL1 on MYPT1 (Thr696) phosphorylation and ROCK1 protein were measured by western blotting in NPC cells after overexpression or knockdown of circRILPL1. **F** The expressions of p-MYPT1 (Thr696), ROCK1, p-YAP (Ser127 and Ser397), YAP, p-LATS1, and LATS1 were measured in the circRILPL1 overexpressed NPC cells treated with the ROCK1 inhibitor Y27632 (10 uM) for 2 h. **G** The expressions of p-MYPT1 (Thr696), ROCK1, p-YAP (Ser127 and Ser397), YAP, p-LATS1, and LATS1 were measured in NPC cells after co-transfection of the circRILPL1 overexpression plasmid and ROCK1 siRNA by western blotting. The average of 3 independent data were presented.

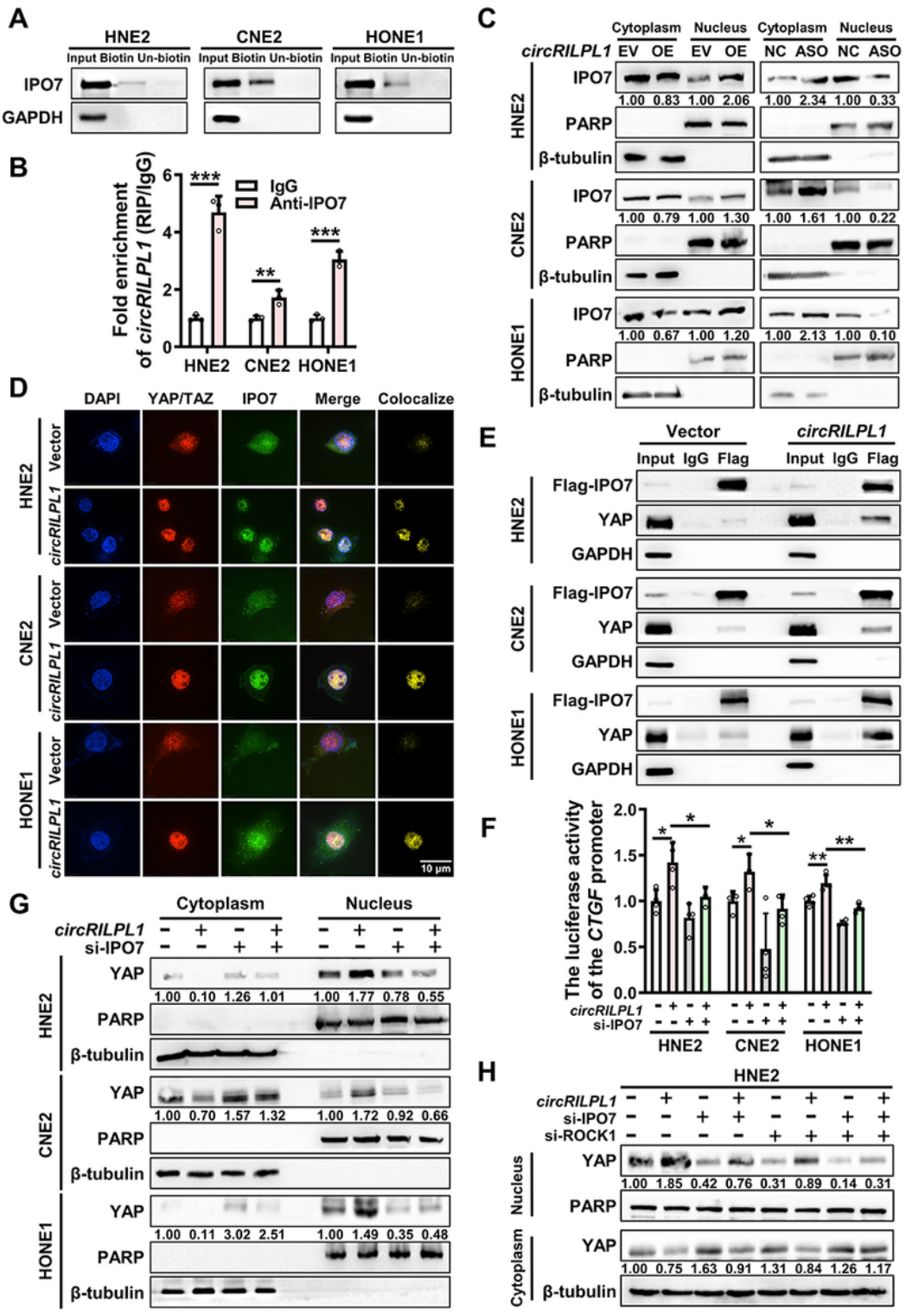

Figure 7

CircRILPL1 promotes YAP nuclear translocation through mediating its binding to IPO7.

A The binding between circRILPL1 and IPO7 protein was detected in NPC cells by RNA pull-down with biotin-labeled circRILPL1 probe. GAPDH was used as a negative control. **B** The binding between circRILPL1 and IPO7 protein was examined in NPC cells using anti-IPO7 antibody by RIP assay. The fold

enrichment of circRILPL1 is relative to that of the control IgG. **, $p < 0.01$; ***, $p < 0.001$. **C** CircRILPL1 promotes the nuclear translocation of IPO7 in NPC cells as examined by cytosolic/nuclear protein fractionation. PARP was used as a nuclear marker and β-tubulin as a cytoplasmic marker. **D** Co-localization of YAP and IPO7 in NPC cells after overexpression of circRILPL1. DAPI: blue; YAP/TAZ: red; IPO7: green; Scale bar = 10 μm. **E** The effect of circRILPL1 on the interaction between YAP and IPO7 was detected by immunoprecipitation using anti-Flag (IPO7) antibody, followed by western blotting using YAP antibody in NPC cells transfected with Flag-IPO7 plasmid, co-transfected with circRILPL1 overexpression plasmid or empty vector. GAPDH was used as a negative control. **F** The transcriptional activity of YAP was measured by luciferase reporter assay after overexpression or knockdown of circRILPL1 or IPO7 in NPC cells. *, $p < 0.05$; **, $p < 0.01$. **G** Knockdown of IPO7 blocked the nuclear import of YAP induced by circRILPL1 in NPC cells. PARP was used as a nuclear marker and β-tubulin as a cytoplasmic marker. **H** Effects of knockdown of IPO7 or ROCK1 on circRILPL1-induced YAP nuclear translocation in NPC cells. The average of 3 independent data were presented.

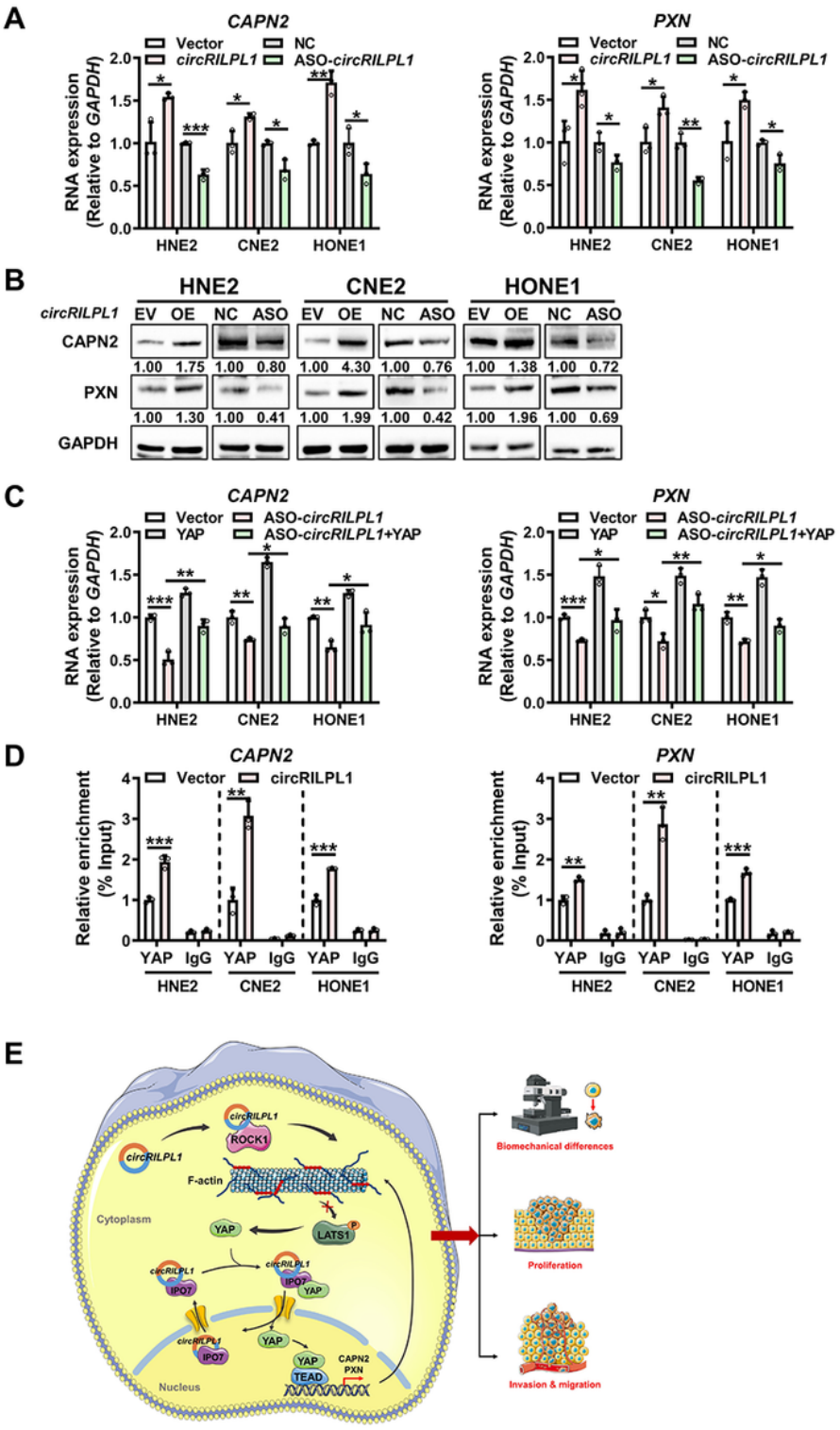

Figure 8

CircRILPL1-YAP signaling promotes the transcription of CAPN2 and PXN.

A The expressions of CAPN2 and PXN mRNA were examined by qRT-PCR in NPC cells after overexpression or knockdown of circRILPL1. Data are presented as the means ± SD. *, $p < 0.05$; **, $p < 0.01$; ***, $p < 0.001$. **B** The expressions of CAPN2 and PXN protein were examined by western blotting in

NPC cells after overexpression or knockdown of circRILPL1. **C** The effects of circRILPL1 and YAP on the expressions of CAPN2 and PXN mRNA in NPC cells were detected by qRT-PCR. Data are presented as the means ± SD. *, $p < 0.05$; **, $p < 0.01$; ***, $p < 0.001$. **D** The effect of circRILPL1 on the enrichment of YAP on CAPN2 and PXN promoters was examined by ChIP assay. Data are presented as the means ± SD. **, $p < 0.01$; ***, $p < 0.001$. **E** Schematic diagram of the signaling pathways regulated by circRILPL1 in NPC cells. CircRILPL1 inhibits the LATS1 kinase through binding to and activating ROCK1, thereby suppressed the phosphorylation of YAP. In cooperation with the nuclear transport receptor IPO7, circRILPL1 prompts loading of YAP onto IPO7 and thus enhances YAP translocation into nucleus, where YAP activates the transcription of cytoskeleton remodeling genes CAPN2 and PXN. CircRILPL1 activates the YAP/HIPPO signaling pathway, ultimately resulting in biomechanical differences, proliferation, and metastasis of NPC cells.

Supplementary Files

This is a list of supplementary files associated with this preprint. Click to download.

- figureS1.jpg
- figureS2.jpg
- figureS3.jpg
- figureS4.jpg
- figureS5.jpg
- figureS6.jpg
- figureS7.jpg
- figureS8.jpg
- SupplementalTable1.xlsx
- SupplementalTable2.xlsx
- SupplementalTable3.xlsx
- SupplementalTable4.xlsx
- SupplementalTable5.xlsx
- SupplementalTable6.xlsx
- SupplementalTable7.xlsx
- SupplementalTable8.xlsx